Computer Modeling in Engineering & Sciences

Tech Science Press

DOI: 10.32604/cmes.2023.024940

check for updates

ARTICLE

Performance Analysis of RIS Assisted NOMA Networks over Rician Fading Channels

Xianli Gong[1], Chongwen Huang[2,3,4], Xinwei Yue[5], Zhaohui Yang[2,4,6] and Feng Liu[1,*]

[1]School of Electronic and Information Engineering, Beihang University, Beijing, 100191, China

[2]College of Information Science and Electronic Engineering, Zhejiang University, Hangzhou, 310027, China

[3]International Joint Innovation Center, Zhejiang University, Haining, 314400, China

[4]Zhejiang Provincial Key Laboratory of Information Processing, Communication and Networking (IPCAN), Hangzhou, 310027, China

[5]School of Information and Communication Engineering, Beijing Information Science and Technology University, Beijing, 100101, China

[6]Zhejiang Laboratory, Hangzhou, 311121, China

*Corresponding Author: Feng Liu. Email: liuf@buaa.edu.cn

Received: 17 June 2022 Accepted: 15 July 2022

ABSTRACT

In this paper, we consider a downlink non-orthogonal multiple access (NOMA) network assisted by two reconfigurable intelligent surfaces (RISs) over Rician fading channels, in which each user communicates with the base station by the virtue of a RIS to enhance the reliability of the received signal. To evaluate the system performance of our proposed RIS-NOMA network, we first derive the exact and asymptotic expressions for the outage probability and ergodic rate of two users. Then, we derive the exact and asymptotic upper bound expressions for the ergodic rate of the nearby user. Based on asymptotic analytical results, the diversity orders for the outage probability and the high signal-to-noise ratio (SNR) slopes for the ergodic rate of the two users are obtained in the high SNR regime. Moreover, we derive the system throughputs of the proposed RIS-NOMA network in delay-limited and delay-tolerant transmission modes. Numerical results confirm our analysis and demonstrate that: 1) The outage probability and ergodic rate of RIS-NOMA networks are superior to that of RIS-assisted orthogonal multiple access (OMA) networks; 2) The RIS-NOMA networks have ability to achieve a larger system throughput compared to RIS-OMA networks; and 3) The system performance of RIS-NOMA networks can be significantly improved as the number of reflecting elements and Rician factor increases.

KEYWORDS

Non-orthogonal multiple access; reconfigurable intelligent surface; outage probability; ergodic rate

1 Introduction

As a promising multiple access technology in the next generation wireless communication network, non-orthogonal multiple access (NOMA) has the ability to tremendously enhance the spectral

and energy efficiency [1,2]. The distinguishing feature of NOMA is that multiple users with different quality-of-service requirements are served by exploiting the superposition coding scheme in the same time/frequency/code resource block [3–5]. In [6,7], the authors have proved that the outage probability and ergodic rate of NOMA can be better than that of conventional orthogonal multiple access (OMA). Zhu et al. [8] have proposed an optimal power allocation scheme learned by adopting the deep deterministic policy gradient algorithm in multiple-input multiple-output NOMA vehicular edge computing.

Recently, reconfigurable intelligent surface (RIS) has been regarded as a promising technology for the next generation wireless communication, which can improve the spectral and energy efficiency of future wireless communication networks in a cost-effective way [9–11]. Specifically, RIS is a low-cost planar array composed of a large number of reconfigurable passive elements, in which the amplitude and phase of the incident signal for each element can be changed independently [12,13]. By adjusting the amplitude and phase coefficients of RIS elements through programmable controller, the electromagnetic signal can be reconfigured to significantly enhance the signal quality and the coverage of wireless communication [14]. Compared with the conventional relaying technology, the advantage of RIS is that the passive reflection does not consume energy and it does not generate self-interference in full duplex (FD) mode [15]. The RIS-empowered multiuser uplink communication system has been investigated in [16], in which a channel estimation framework based on the parallel factor decomposition has been proposed to unfold the resulting cascaded channel model. In [17], the authors have studied the downlink wireless communication system, in which the transmit beamforming and the RIS have been jointly optimized to maximize the energy efficiency of the system. A new joint design of the transmit beamforming and the phase shifting of the RIS has been proposed in [18], in which the sum rate of the multiuser system has been maximized by using deep reinforcement learning (DRL). In [19], the multiuser communication system assisted by RIS has been considered, in which the power allocation and the phase shifting of the RIS have been jointly optimized to minimize the sum transmit power. Considering RIS-empowered terahertz band communications, a DRL-based hybrid beamforming scheme has been proposed in [20] to improve the communication coverage.

1.1 Related Work

Since both RIS and NOMA can greatly improve the spectrum and energy efficiency, it is critical to study their combined advantages to further enhance the spectrum and energy efficiency of future wireless communication networks. In [21], a simple RIS-NOMA transmission scheme has been designed, in which the outage performance of the cell-edge user has been improved with the assistance of RIS in a NOMA system. In [22], the authors have investigated the performance of RIS-NOMA networks in terms of the outage probability, ergodic rate, and energy efficiency by exploiting 1-bit coding scheme. The effects of coherent phase shifting and random phase shifting on outage performance for RIS-NOMA networks have been investigated in [23]. By designing the passive beamforming weights, the authors in [24] have investigated the outage probability and ergodic rate of prioritized user for RIS-NOMA. The RIS reflection with discrete phase shifting for RIS-NOMA and RIS-OMA has been analyzed in [25]. In [26], a novel NOMA solution with RIS partitioning has been proposed to reduce the transmission interference. Considering the impact of the direct link from the base station (BS) to users on the network performance, the outage behaviors of multiple RISs-assisted NOMA networks have been studied by using discrete phase shifting in [27]. The authors in [28] have examined the outage performance of RIS-NOMA networks under presence of hardware impairment. In [29], the outage probability and ergodic rate of RIS-aided uplink and downlink NOMA networks have been investigated by employing continuous phase shifting. The authors in [30] have studied RIS

assisted downlink NOMA networks, in which the performance of the networks has been analyzed by using the coherent phase shifting.

1.2 Motivation and Contributions

As mentioned in the above works, compared with the conventional relaying technology, the RIS is capable of reflecting the incident signal transmitted from the transmitter to the receiver in FD mode without self-interference and energy consumption, which not only enhances the spectrum and energy efficiency, but also has a very low cost. Therefore, the integration of RIS and NOMA can further improve the spectrum and energy efficiency of the next generation wireless communication networks. Furthermore, the current literature on RIS-NOMA mainly concentrates on the optimization problem, but the research on performance analysis is not enough. Compared with conventional NOMA systems, the performance analysis of RIS-NOMA systems is more complex and challenging owing to the influence of the RIS. These motivate us to study the performance of RIS assisted NOMA systems, which provides an important theoretical basis for deployment of RIS in the future.

In this paper, we consider a RIS assisted NOMA network, in which a pair of NOMA users in a cell cannot directly receive signals from the BS due to the obstruction of obstacles, and each user needs the help of a RIS. Moreover, we comprehensively analyze the performance of RIS-NOMA networks in terms of the outage probability, ergodic rate, and system throughput. The primary contributions of this paper are summarized as follows:

- We derive the closed-form and asymptotic expressions for the outage probability of a pair of NOMA users over Rician fading channels for the proposed RIS-assisted NOMA network. To gain further insight, we obtain the diversity orders of the pair of NOMA users for RIS-NOMA network according to the asymptotic analyses at high signal-to-noise ratio (SNR). We observe that the diversity orders of the pair of NOMA users depend on the number of reflecting elements and Rician factor.
- We compare the outage performance of the pair of users for RIS-NOMA and RIS-OMA networks. We demonstrate that the outage performance of RIS-NOMA outperforms that of RIS-OMA. We prove that the RIS-NOMA network is capable of improving outage performance with increasing the number of reflecting elements and Rician factor.
- We derive the exact and asymptotic expressions for the ergodic rate of the pair of NOMA users over Rician fading channels for our proposed RIS-NOMA network. To approximate the exact ergodic rate, we also derive the exact and asymptotic upper bound expressions for the ergodic rate of the nearby user. Based on theoretical analyses, we obtain the high SNR slopes for the ergodic rate of the pair of NOMA users. We observe that the throughput ceiling appears in the ergodic rate of the distant user at high SNR. We demonstrate that the superiority of RIS-NOMA over RIS-OMA in terms of the ergodic rate. We evidence that the ergodic rate of RIS-NOMA becomes larger with the increase of the number of reflecting elements.
- We analyze the system throughput of our proposed RIS-NOMA network in two transmission modes. In delay-limited transmission mode, we observe that the system throughput of RIS-NOMA converges to a constant at high SNR. Furthermore, we prove that the proposed RIS-NOMA is capable of enhancing the system throughput compared to RIS-OMA. In delay-tolerant transmission mode, we evidence that the proposed RIS-NOMA can achieve a larger system throughput than RIS-OMA at high SNR. Moreover, we confirm that as the number of reflecting elements increases, the system throughput of RIS-NOMA can be significantly improved in the two transmission modes.

The main notations used in this paper are explained as follows. $\mathbb{C}^{x\times y}$ denotes the space of $x \times y$ complex-valued matrices. V^H represents the conjugate-transpose of V. $f_X(\cdot)$ and $F_X(\cdot)$ mean the probability density function (PDF) and cumulative distribution function (CDF) of random variable X, respectively. diag $(\cdot)$ denotes a diagonal matrix. Pr $(\cdot)$ denotes the probability. $\mathbb{E}(\cdot)$ and $\mathbb{D}(\cdot)$ stand for the expectation and variance, respectively.

2 System Model

Consider a two-RIS assisted NOMA network with one single-antenna BS and two single-antenna users as shown in Fig. 1, in which the BS sends the superposed signals to the pair of NOMA users by means of two RISs. Assume that there is no direct link between the BS and each NOMA user due to strong attenuation, and each NOMA user needs a RIS to assist in communicating with the BS. D_1 and D_2 are the nearby user and the distant user, respectively. R_1 and R_2 are RISs corresponding to D_1 and D_2, respectively. Each RIS has K reflecting elements. The reflecting phase shifting matrix of R_n is denoted by $\vartheta_n = \text{diag}(\beta e^{j\theta_n^1}, \ldots, \beta e^{j\theta_n^k}, \ldots, \beta e^{j\theta_n^K})$, $n \in \{1, 2\}$, where $\beta \in [0, 1]$ and $\theta_n^k \in [0, 2\pi)$ represent the amplitude coefficient and the phase shift of the k-th reflecting element of the RIS, respectively.

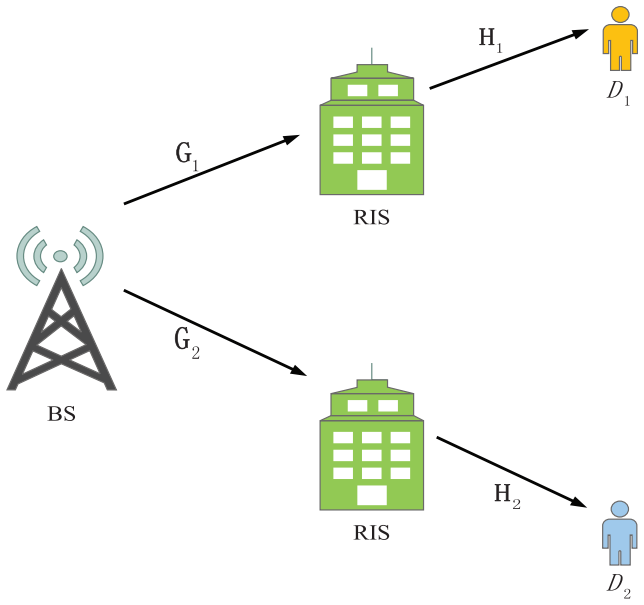

Figure 1: System model of RIS assisted downlink NOMA networks

2.1 Channel Model

It is assumed that the channel state information of all channels is completely known at the BS. The complex channel coefficients from the BS to R_n and from R_n to D_n are represented by $\mathbf{G}_n \in \mathbb{C}^{K\times 1}$ and $\mathbf{H}_n \in \mathbb{C}^{K\times 1}$, respectively. Assume that the wireless links for RIS-NOMA networks are modeled as Rician fading channels. The cascade channel gains from the BS to R_n and from R_n to D_n can be expressed as $\mathbf{H}_n^H \vartheta_n \mathbf{G}_n$. The channel coefficient matrixes can be written as

$$\mathbf{G}_n = [G_n^1, \ldots, G_n^k, \ldots, G_n^K]^H, \tag{1}$$

and

$$\mathbf{H}_n = [H_n^1, \ldots, H_n^k, \ldots, H_n^K]^H, \tag{2}$$

where the channel coefficients from the BS to the k-th reflecting element of R_n and from the k-th reflecting element of R_n to D_n are respectively given by

$$G_n^k = \sqrt{\alpha_{n,1}^k}\left(\sqrt{\frac{\kappa}{\kappa+1}} + \sqrt{\frac{1}{\kappa+1}}\widetilde{G}_n^k\right), \tag{3}$$

and

$$H_n^k = \sqrt{\alpha_{n,2}^k}\left(\sqrt{\frac{\kappa}{\kappa+1}} + \sqrt{\frac{1}{\kappa+1}}\widetilde{H}_n^k\right). \tag{4}$$

Defining $\alpha_{n,1}^k = \eta d_{n,1}^{-\alpha}$, $\alpha_{n,2}^k = \eta d_{n,2}^{-\alpha}$, $d_{n,1}$ and $d_{n,2}$ are the distances from the BS to R_n and from R_n to D_n, respectively. κ, α, and η are the Rician factor, path loss exponent, and frequency dependent factor, respectively. The fading gains $\widetilde{G}_n^k$ and $\widetilde{H}_n^k$ follow complex Gaussian distribution with zero mean and unit variance, i.e., $\widetilde{G}_n^k \sim \mathscr{CN}(0,1)$ and $\widetilde{H}_n^k \sim \mathscr{CN}(0,1)$.

2.2 Signal Model

Based on the superposition coding scheme, the BS broadcasts superposed signal $s = \sqrt{a_1 P_b}s_1 + \sqrt{a_2 P_b}s_2$ to D_1 and D_2, where P_b means the normalized transmit power of the BS, s_n represents the unit power signal transmitted to D_n with a_n denoting the power allocation factor of D_n. For simplicity, we assume a fixed power allocation between two users. The optimized power sharing between non-orthogonal users can further enhance the system performance of RIS-NOMA networks, which will be studied in future work. For user fairness, the power allocation factor satisfies $a_2 > a_1$ with $a_1 + a_2 = 1$. The received signals at D_1 and D_2 are respectively given by

$$y_{D_1} = \mathbf{H}_1^H \vartheta_1 \mathbf{G}_1 \left(\sqrt{a_1 P_b}s_1 + \sqrt{a_2 P_b}s_2\right) + n_{D_1}, \tag{5}$$

and

$$y_{D_2} = \mathbf{H}_2^H \vartheta_2 \mathbf{G}_2 \left(\sqrt{a_1 P_b}s_1 + \sqrt{a_2 P_b}s_2\right) + n_{D_2}, \tag{6}$$

where n_{D_n} represents the additive white Gaussian noise with the mean power N_0 at D_n. On the basis of the successive interference cancellation (SIC) principle, the signal of D_2 is detected first at D_1. The received signal-to-interference-plus-noise ratio (SINR) at D_1 to detect signal s_2 of D_2 is given by

$$\gamma_{D_1 \to s_2} = \frac{\rho \left|\mathbf{H}_1^H \vartheta_1 \mathbf{G}_1\right|^2 a_2}{\rho \left|\mathbf{H}_1^H \vartheta_1 \mathbf{G}_1\right|^2 a_1 + 1}, \tag{7}$$

where $\rho = \dfrac{P_b}{N_0}$ is the transmit SNR. After performing SIC, the signal of D_1 is detected at D_1. The received SINR of detecting signal s_1 of D_1 at D_1 can be given by

$$\gamma_{D_1 \to s_1} = \rho \left|\mathbf{H}_1^H \vartheta_1 \mathbf{G}_1\right|^2 a_1. \tag{8}$$

The signal of D_2 is directly detected by treating the signal of D_1 as interference at D_2. The received SINR of D_2 to detect its own signal can be given by

$$\gamma_{D_2 \to s_2} = \frac{\rho \left| \mathbf{H}_2^H \vartheta_2 \mathbf{G}_2 \right|^2 a_2}{\rho \left| \mathbf{H}_2^H \vartheta_2 \mathbf{G}_2 \right|^2 a_1 + 1}. \tag{9}$$

2.3 RIS-OMA

For comparison, we regard the RIS-OMA scheme as the benchmark, in which the BS sends information to two OMA users through two RISs in two time slots. In each time slot, signal s_n is transmitted from the BS to D_n by utilizing R_n. The observation at D_n is given by

$$y_{n,D_n}^{\text{OMA}} = \mathbf{H}_n^H \vartheta_n \mathbf{G}_n \sqrt{P_b} s_n + n_{D_n}. \tag{10}$$

The received SINR at D_n for detecting its own signal can be given by

$$\gamma_{n,D_n \to s_n}^{\text{OMA}} = \rho \left| \mathbf{H}_n^H \vartheta_n \mathbf{G}_n \right|^2. \tag{11}$$

2.4 Channel Statistics

In order to achieve optimal performance, we use the coherent phase shift design. For the wireless communication links of RIS-NOMA networks, our goal is to optimize the channel by adjusting the amplitude and phase of the RIS to achieve the optimal channel gain for each user. For the BS-RIS-D_n link, we maximize $\left| \mathbf{H}_n^H \vartheta_n \mathbf{G}_n \right| = \left| \sum_{k=1}^{K} \beta G_n^k H_n^k e^{j\theta_n^k} \right|$, where G_n^k and H_n^k are the k-th element of $\mathbf{G}_n$ and $\mathbf{H}_n$, respectively. In order to achieve maximization, the sum of the phase of $G_n^k H_n^k$ and the phase shift θ_n^k of the k-th reflecting element of the RIS is equal to zero. Therefore, we have

$$\left| \mathbf{H}_n^H \vartheta_n \mathbf{G}_n \right| = \sum_{k=1}^{K} \left| G_n^k H_n^k \right|, \tag{12}$$

where $\beta = 1$ without loss of generality.

The channel coefficients G_n^k from the BS to the k-th reflecting element and H_n^k from the k-th reflecting element to D_n follow Rician distribution, hence the probability density function (PDF) of cascade Rician channel $X_n^k = \left| G_n^k H_n^k \right|$ in [31] is expressed as

$$f_{X_n^k}(x) = \frac{1}{\sqrt{\alpha_{n,1}\alpha_{n,2}}} \sum_{i=0}^{\infty} \sum_{j=0}^{\infty} \frac{4x^{i+j+1}(\kappa+1)^{i+j+2}\kappa^{i+j}}{(i!)^2 (j!)^2 e^{2\kappa}} \left(\alpha_{n,1}\alpha_{n,2}\right)^{-\frac{i+j+1}{2}} K_{i-j}\left[\frac{2x(\kappa+1)}{\sqrt{\alpha_{n,1}\alpha_{n,2}}}\right], \tag{13}$$

where $K_\nu(\cdot)$ denotes the modified Bessel function of the second kind with order ν [32]. The mean and variance of X_n^k are respectively written as

$$\mu_n = \mathbb{E}\left(X_n^k\right) = \frac{\pi \sqrt{\alpha_{n,1}\alpha_{n,2}}}{4(1+\kappa)} \left[L_{\frac{1}{2}}(-\kappa)\right]^2, \tag{14}$$

and

$$\Omega_n = \mathbb{D}\left(X_n^k\right) = \alpha_{n,1}\alpha_{n,2} \left\{1 - \frac{\pi^2}{16(1+\kappa)^2} \left[L_{\frac{1}{2}}(-\kappa)\right]^4\right\}, \tag{15}$$

where $L_{\frac{1}{2}}(\cdot)$ represents the Laguerre polynomial and $L_{\frac{1}{2}}(\kappa) = e^{\frac{1}{2}\kappa}\left[(1-\kappa) K_0\left(-\frac{\kappa}{2}\right) - \kappa K_1\left(-\frac{\kappa}{2}\right)\right]$.

3 Outage Probability

In communication systems, the outage probability can be defined as the probability that the outage occurs for a user when the information rate of the user is lower than its target rate. The outage probability is a widely used system performance metric in fixed-rate transmission systems. In this section, the outage performance of downlink RIS-NOMA networks is investigated.

3.1 Outage Probability of D_1

By using the SIC scheme at nearby user D_1, the signal of distant user D_2 is detected first, and then its own signal is detected. Therefore, when both signals s_1 and s_2 cannot be successfully detected by D_1, an outage occurs for D_1. Based on Eqs. (7) and (8), the outage probability of D_1 for RIS-NOMA networks can be expressed as

$$P_{D_1} = 1 - \Pr\left(\gamma_{D_1 \to s_1} > \gamma_{th_1}, \gamma_{D_1 \to s_2} > \gamma_{th_2}\right), \tag{16}$$

where $\gamma_{th_1} = 2^{r_1} - 1$ and $\gamma_{th_2} = 2^{r_2} - 1$ represent the target SNRs with r_1 and r_2 denoting the target rates of D_1 and D_2 to detect signals s_1 and s_2, respectively. The outage probability of D_1 is derived in the following theorem.

Theorem 3.1. Under Rician fading channels, the closed-form expression for the outage probability of D_1 for RIS-NOMA networks can be approximated as

$$P_{D_1} \approx \frac{1}{\Gamma\left(\frac{K\mu_1^2}{\Omega_1}\right)} \gamma\left(\frac{K\mu_1^2}{\Omega_1}, \frac{\mu_1\sqrt{\lambda}}{\Omega_1}\right), \tag{17}$$

where $\lambda \triangleq \max(\lambda_1, \lambda_2)$, $\lambda_1 = \dfrac{\gamma_{th_1}}{\rho a_1}$, $\lambda_2 = \dfrac{\gamma_{th_2}}{\rho(a_2 - a_1\gamma_{th_2})}$ with $a_2 > a_1\gamma_{th_2}$, $\mu_1 = \dfrac{\pi\sqrt{\alpha_{1,1}\alpha_{1,2}}}{4(1+\kappa)}\left[L_{\frac{1}{2}}(-\kappa)\right]^2$, $\Omega_1 = \alpha_{1,1}\alpha_{1,2}\left\{1 - \dfrac{\pi^2}{16(1+\kappa)^2}\left[L_{\frac{1}{2}}(-\kappa)\right]^4\right\}$, $\gamma(\alpha, x) = \int_0^x e^{-t}t^{\alpha-1}dt$ is the lower incomplete Gamma function [32], and $\Gamma(z) = \int_0^\infty e^{-t}t^{z-1}dt$ is the gamma function [32].

Proof: See Appendix A.

Remark 3.1. From Eq. (17), it is observed that the approximate outage probability of D_1 for RIS-NOMA is subject to ρ, K, κ, and α when the target SNR and the power allocation coefficient are fixed. Specifically, increasing ρ, K, κ, and α, the approximate outage probability of D_1 for RIS-NOMA decreases. As a result, the outage performance of D_1 for RIS-NOMA can be enhanced.

3.2 Outage Probability of D_2

On account of the NOMA principle, the signal of D_2 is directly detected at distant user D_2. Thus the outage occurs for D_2 when signal s_2 cannot be successfully detected by D_2. In view of Eq. (9), the outage probability of D_2 for RIS-NOMA networks can be expressed as

$$P_{D_2} = \Pr\left(\gamma_{D_2 \to s_2} < \gamma_{th_2}\right). \tag{18}$$

The outage probability of D_2 is derived in the following theorem.

Theorem 3.2. Under Rician fading channels, the closed-form expression for the outage probability of D_2 for RIS-NOMA networks can be approximated as

$$P_{D_2} \approx \frac{1}{\Gamma\left(\frac{K\mu_2^2}{\Omega_2}\right)}\gamma\left(\frac{K\mu_2^2}{\Omega_2}, \frac{\mu_2\sqrt{\lambda_2}}{\Omega_2}\right), \tag{19}$$

where $\mu_2 = \frac{\pi\sqrt{\alpha_{2,1}\alpha_{2,2}}}{4\,(1+\kappa)}\left[L_{\frac{1}{2}}\,(-\kappa)\right]^2$ and $\Omega_2 = \alpha_{2,1}\alpha_{2,2}\left\{1 - \frac{\pi^2}{16(1+\kappa)^2}\left[L_{\frac{1}{2}}\,(-\kappa)\right]^4\right\}$.

Proof: See Appendix B.

Remark 3.2. From Eq. (19), it can be seen that the approximate outage probability of D_2 for RIS-NOMA depends on ρ, K, κ, and α. Similarly, as ρ, K, κ, and α increase, the approximate outage probability of D_2 for RIS-NOMA decreases. Consequently, the outage performance of D_2 for RIS-NOMA can be improved.

3.3 Outage Probability of D_n for RIS-OMA

For RIS-OMA networks, D_n detects its own signal s_n in each time slot. Hence the outage occurs for D_n when its own signal cannot be successfully detected. According to Eq. (11), the outage probability of D_n for RIS-OMA networks can be expressed as

$$P_{D_n}^{\mathrm{OMA}} = \Pr\left(\gamma_{n,D_n\to s_n}^{\mathrm{OMA}} < \gamma_{th_n}^{\mathrm{OMA}}\right), \tag{20}$$

where $\gamma_{th_n}^{\mathrm{OMA}} = 2^{2r_n^{\mathrm{OMA}}} - 1$ is the target SNR with r_n^{OMA} being the target rate of D_n to detect signal s_n. The derivation process of the outage probability for RIS-OMA networks is similar to that of RIS-NOMA networks. The outage probability of D_n for RIS-OMA networks can be provided in the following corollary.

Corollary 3.1. Under Rician fading channels, the closed-form expression for the outage probability of D_n for RIS-OMA networks can be approximated as

$$P_{D_n}^{\mathrm{OMA}} \approx \frac{1}{\Gamma\left(\frac{K\mu_n^2}{\Omega_n}\right)}\gamma\left(\frac{K\mu_n^2}{\Omega_n}, \frac{\mu_n\sqrt{\tau_n}}{\Omega_n}\right), \tag{21}$$

where $\tau_n = \frac{\gamma_{th_n}^{\mathrm{OMA}}}{\rho}$.

3.4 Diversity Analysis

In communication systems, the diversity order can be defined as the slope of the outage probability at high SNR. The diversity order describes the speed at which the outage probability decreases with the transmit SNR, which is usually used to evaluate the outage performance of wireless communication networks. The diversity order can be expressed as

$$d = -\lim_{\rho\to\infty}\frac{\log\left(P_D^{\infty}(\rho)\right)}{\log(\rho)}. \tag{22}$$

In order to obtain further insights, the approximate results of the outage probability are analyzed at high SNR, which can be used to determine the diversity order. The asymptotic outage probabilities of D_1 and D_2 at high SNR for RIS-NOMA networks can be provided in the following corollary.

Corollary 3.2. Based on Eqs. (17) and (19), when $\rho \to \infty$, the asymptotic expressions for outage probability of D_1 and D_2 for RIS-NOMA networks can be respectively given by

$$P_{D_1}^{\infty} \approx \frac{\Omega_1}{K\mu_1^2} \frac{1}{\Gamma\left(\frac{K\mu_1^2}{\Omega_1}\right)} \left(\frac{\mu_1\sqrt{\lambda}}{\Omega_1}\right)^{\frac{K\mu_1^2}{\Omega_1}}, \tag{23}$$

and

$$P_{D_2}^{\infty} \approx \frac{\Omega_2}{K\mu_2^2} \frac{1}{\Gamma\left(\frac{K\mu_2^2}{\Omega_2}\right)} \left(\frac{\mu_2\sqrt{\lambda_2}}{\Omega_2}\right)^{\frac{K\mu_2^2}{\Omega_2}}. \tag{24}$$

Proof: Applying the series representation [32], when $\rho \to \infty$, we have $\lambda \to 0$ and $\lambda_2 \to 0$, by extracting the first term ($n = 0$) of series representation, the high SNR approximate expressions can be given by

$$\gamma\left(\frac{K\mu_1^2}{\Omega_1}, \frac{\mu_1\sqrt{\lambda}}{\Omega_1}\right) \approx \frac{\Omega_1}{K\mu_1^2} \left(\frac{\mu_1\sqrt{\lambda}}{\Omega_1}\right)^{\frac{K\mu_1^2}{\Omega_1}}, \tag{25}$$

and

$$\gamma\left(\frac{K\mu_2^2}{\Omega_2}, \frac{\mu_2\sqrt{\lambda_2}}{\Omega_2}\right) \approx \frac{\Omega_2}{K\mu_2^2} \left(\frac{\mu_2\sqrt{\lambda_2}}{\Omega_2}\right)^{\frac{K\mu_2^2}{\Omega_2}}. \tag{26}$$

Substituting Eqs. (25) and (26) into Eqs. (17) and (19), respectively, Eqs. (23) and (24) can be obtained. The proof is completed.

Remark 3.3. From Eqs. (23) and (24), it can be observed that the asymptotic outage probabilities of D_1 and D_2 for RIS-NOMA are related to ρ, K, κ, and α. Hence the asymptotic outage probabilities of D_1 and D_2 for RIS-NOMA increase with the increase of ρ, K, κ, and α at high SNR.

Substituting Eqs. (23) and (24) into Eq. (22), the diversity orders of D_1 and D_2 for RIS-NOMA networks can be respectively calculated as

$$d_{D_1} = -\lim_{\rho\to\infty} \frac{\log\left(P_{D_1}^{\infty}(\rho)\right)}{\log(\rho)} = \frac{K\mu_1^2}{2\Omega_1}, \tag{27}$$

and

$$d_{D_2} = -\lim_{\rho\to\infty} \frac{\log\left(P_{D_2}^{\infty}(\rho)\right)}{\log(\rho)} = \frac{K\mu_2^2}{2\Omega_2}. \tag{28}$$

Remark 3.4. From Eqs. (27) and (28), we can observe that the diversity orders of D_1 and D_2 for RIS-NOMA are influenced by the number of reflecting elements of RIS, the Rician factor, and the path loss exponent.

Remark 3.5. It can be observed that the diversity orders increase as K, κ, and α increase. The outage probability curve becomes steeper with the increase of the diversity order, resulting in the faster convergence of the outage probability. Therefore, increasing the diversity order can improve the outage performance of RIS-NOMA at high SNR.

Remark 3.6. Similarly, the diversity order of D_n for RIS-OMA is $\frac{K\mu_n^2}{2\Omega_n}$, which is also in connection with K, κ, and α.

3.5 Delay-Limited System Throughput

The system throughput is an important performance metric in wireless communication systems. The research on system throughput is of great significance for practical implementation. In the delay-limited transmission mode, the information is transmitted from the BS to users at a constant rate, which leads to outage due to the influence of the wireless fading channels. Therefore, the system throughput depends on the outage probability in the delay-limited transmission mode. The delay-limited system throughput of RIS-NOMA is expressed as

$$R_{DL} = \left(1 - P_{D_1}\right) r_1 + \left(1 - P_{D_2}\right) r_2, \tag{29}$$

where P_{D_1} and P_{D_2} are the outage probabilities from Eqs. (17) and (19), respectively.

4 Ergodic Rate

The ergodic rate is a commonly used system performance metric in adaptive-rate transmission systems. In this section, the ergodic rates of two users for RIS-NOMA networks are analyzed.

4.1 Ergodic Rate of D_1

Based on SIC principle, if D_1 can successfully detect the signal of D_2, the achievable rate of D_1 can be given by $R_{D_1} = \log\left(1 + \gamma_{D_1 \to s_1}\right)$. On account of Eq. (8), the ergodic rate of D_1 for RIS-NOMA networks is expressed as

$$R_{D_1}^{erg} = \mathbb{E}\left[\log\left(1 + \gamma_{D_1 \to s_1}\right)\right]. \tag{30}$$

The ergodic rate of D_1 is obtained in the following theorem.

Theorem 4.1. Under Rician fading channels, the exact expression for the ergodic rate of D_1 for RIS-NOMA is calculated as

$$R_{D_1}^{erg} = \frac{\rho a_1}{\ln 2} \int_0^{\infty} \frac{\Gamma\left(\omega_1 + 1\right) - \gamma\left(\omega_1 + 1, \frac{\sqrt{y}}{\upsilon_1}\right)}{\left(1 + \rho a_1 y\right)\Gamma\left(\omega_1 + 1\right)} dy, \tag{31}$$

where $\omega_1 = \frac{K\mu_1^2}{\Omega_1} - 1$ and $\upsilon_1 = \frac{\Omega_1}{\mu_1}$.

Proof: See Appendix C.

Remark 4.1. From Eq. (31), we can observe that the ergodic rate of D_1 for RIS-NOMA is dependent on ρ, K, κ, and α when the target SNR and the power allocation coefficient are constants. More specifically, with the increase of ρ, K, κ, and α, the ergodic rate of D_1 for RIS-NOMA increases.

4.2 Ergodic Rate of D_2

Assuming that D_2 can detect its own signal s_2, the achievable rate of D_2 can be given by $R_{D_2} = \log\left(1 + \gamma_{D_2 \to s_2}\right)$. In virtue of Eq. (9), the ergodic rate of D_2 for RIS-NOMA networks is expressed as

$$R_{D_2}^{erg} = \mathbb{E}\left[\log\left(1 + \gamma_{D_2 \to s_2}\right)\right]. \tag{32}$$

The ergodic rate of D_2 is obtained in the following theorem.

Theorem 4.2. Under Rician fading channels, the approximate expression for the ergodic rate of D_2 for RIS-NOMA is calculated as

$$R_{D_2}^{erg} \approx \frac{\pi}{L \ln 2} \sum_{l=1}^{L} \frac{a_2 \sqrt{1-t_l^2}}{2a_1 + a_2 (t_l + 1)} \left[1 - \frac{1}{\Gamma(\omega_2 + 1)} \gamma \left(\omega_2 + 1, \frac{1}{\upsilon_2} \sqrt{\frac{t_l + 1}{\rho a_1 (1 - t_l)}} \right) \right], \tag{33}$$

where $t_l = \cos\left(\frac{2l-1}{2L}\pi\right)$, $\omega_2 = \frac{K\mu_2^2}{\Omega_2} - 1$, and $\upsilon_2 = \frac{\Omega_2}{\mu_2}$.

Proof: See Appendix D.

Remark 4.2. From Eq. (33), it is observed that the ergodic rate of D_2 for RIS-NOMA is related to ρ, K, κ, and α. Similarly, the ergodic rate of D_2 for RIS-NOMA increases with ρ, K, κ, and α.

4.3 Ergodic Rate of D_n for RIS-OMA

For RIS-OMA networks, since D_n can detect its own signal s_n, the achievable rate of D_n can be given by $R_{D_n,OMA} = \frac{1}{2} \log\left(1 + \gamma_{n,D_n \to s_n}^{\text{OMA}}\right)$. According to Eq. (11), the ergodic rate of D_n for RIS-OMA networks can be expressed as

$$R_{D_n,OMA}^{erg} = \mathbb{E}\left[\frac{1}{2} \log\left(1 + \gamma_{n,D_n \to s_n}^{\text{OMA}}\right) \right]. \tag{34}$$

Similar to the derivation process of Eq. (31), the ergodic rate of D_n can be presented in the following corollary.

Corollary 4.1. Under Rician fading channels, the exact expression for the ergodic rate of D_n for RIS-OMA is given by

$$R_{D_n,OMA}^{erg} = \frac{\rho}{2 \ln 2} \int_0^{\infty} \frac{\Gamma(\omega_n + 1) - \gamma\left(\omega_n + 1, \frac{\sqrt{y}}{\upsilon_n}\right)}{(1 + \rho y)\, \Gamma(\omega_n + 1)} dy. \tag{35}$$

4.4 Slope Analysis

Similar to the diversity order, the high SNR slope can be defined as the slope of the ergodic rate at high SNR, which describes how fast the ergodic rate increases with the transmit SNR. The high SNR slope can be expressed as

$$S = \lim_{\rho \to \infty} \frac{R_{D,erg}^{\infty}(\rho)}{\log(\rho)}. \tag{36}$$

To gain deep insights into the system performance, the approximate ergodic rate at high SNR is studied, which can be used to calculate the high SNR slope. However, the approximate ergodic rate of D_1 at high SNR cannot be obtained from Eq. (31). For the convenience of analyses, the upper bound for the ergodic rate of D_1 can be derived in the following theorem.

Theorem 4.3. Under Rician fading channels, the upper bound for the ergodic rate of D_1 for RIS-NOMA can be calculated as

$$R_{D_1,UB}^{erg} = \log\left(1 + \rho a_1 \left((K\mu_1)^2 + K\Omega_1\right)\right). \tag{37}$$

Proof: Based on Eq. (30), by adopting the Jensen's inequality, the upper bound for the ergodic rate of D_1 can be given by

$$R_{D_1}^{erg} = \mathbb{E}\left[\log\left(1+\left|\mathbf{H}_1^H\vartheta_1\mathbf{G}_1\right|^2\rho a_1\right)\right] \le \log\left(1+\rho a_1\mathbb{E}\left(\left|\mathbf{H}_1^H\vartheta_1\mathbf{G}_1\right|^2\right)\right). \tag{38}$$

On the basis of Eq. (12), the upper bound for the ergodic rate of D_1 can be expressed as

$$R_{D_1,UB}^{erg} = \log\left(1+\rho a_1\mathbb{E}\left(|X_1|^2\right)\right). \tag{39}$$

According to Eqs. (14) and (15), the upper bound for the ergodic rate of D_1 can be calculated as

$$R_{D_1,UB}^{erg} = \log\left(1+\rho a_1\left(\mathbb{E}^2\left(X_1\right)+\mathbb{D}\left(X_1\right)\right)\right) = \log\left(1+\rho a_1\left(\left(K\mu_1\right)^2+K\Omega_1\right)\right). \tag{40}$$

Hence Eq. (37) can be obtained. The proof is completed.

Remark 4.3. From Eq. (37), we can observe that the upper bound for the ergodic rate of D_1 for RIS-NOMA is related to ρ, K, κ, and α. Specifically, the upper bound for the ergodic rate of D_1 for RIS-NOMA increases with ρ, K, κ, and α.

The asymptotic upper bound for the ergodic rate of D_1 at high SNR for RIS-NOMA networks can be provided in the following corollary.

Corollary 4.2. Based on Eq. (37), when $\rho \to \infty$, the asymptotic upper bound for the ergodic rate of D_1 for RIS-NOMA can be given by

$$R_{D_1,UB}^{erg,\infty} = \log\left(\rho a_1\left(\left(K\mu_1\right)^2+K\Omega_1\right)\right). \tag{41}$$

Remark 4.4. From Eq. (41), we can observe that the asymptotic upper bound for the ergodic rate of D_1 for RIS-NOMA depends on ρ, K, κ, and α. Similarly, increasing ρ, K, κ, and α, the asymptotic upper bound for the ergodic rate of D_1 for RIS-NOMA increases at high SNR.

Substituting Eq. (41) into Eq. (36), the high SNR slope of D_1 for RIS-NOMA networks can be calculated as

$$S_{D_1} = \lim_{\rho\to\infty}\frac{R_{D_1,UB}^{erg,\infty}(\rho)}{\log(\rho)} = 1. \tag{42}$$

Remark 4.5. From Eq. (42), we can observe that the high SNR slope of D_1 for RIS-NOMA is a non-zero value. This implies that the ergodic rate of D_1 for RIS-NOMA tends to infinity at high SNR. The higher the high SNR slope, the steeper the ergodic rate curve, which results in the faster convergence of the ergodic rate. Hence the ergodic rate increases with the increase of the high SNR slope.

The asymptotic ergodic rate of D_2 at high SNR for RIS-NOMA networks can be presented in the following corollary.

Corollary 4.3. Based on Eq. (32), when $\rho \to \infty$, the asymptotic ergodic rate of D_2 for RIS-NOMA can be calculated as

$$R_{D_2}^{erg,\infty} = \log\left(1+\frac{a_2}{a_1}\right). \tag{43}$$

Proof: With the aid of Eqs. (9) and (12), we can obtain

$$\lim_{\rho\to\infty}\gamma_{D_2\to s_2}=\lim_{\rho\to\infty}\frac{\rho\left|\mathbf{H}_2^H\vartheta_2\mathbf{G}_2\right|^2a_2}{\rho\left|\mathbf{H}_2^H\vartheta_2\mathbf{G}_2\right|^2a_1+1}=\lim_{\rho\to\infty}\frac{\rho\left|X_2\right|^2a_2}{\rho\left|X_2\right|^2a_1+1}=\frac{a_2}{a_1}. \tag{44}$$

In view of Eq. (32), when $\rho\to\infty$, the asymptotic ergodic rate of D_2 can be calculated as

$$R_{D_2}^{erg,\infty}=\lim_{\rho\to\infty}\mathbb{E}\left[\log\left(1+\gamma_{D_2\to s_2}\right)\right]=\mathbb{E}\left[\log\left(1+\lim_{\rho\to\infty}\gamma_{D_2\to s_2}\right)\right]=\log\left(1+\frac{a_2}{a_1}\right). \tag{45}$$

Hence Eq. (43) can be obtained. The proof is completed.

Remark 4.6. From Eq. (43), it can be observed that the asymptotic ergodic rate of D_2 for RIS-NOMA is a constant when the power allocation coefficient is fixed. Hence the asymptotic ergodic rate of D_2 for RIS-NOMA remains unchanged at high SNR.

Substituting Eq. (43) into Eq. (36), the high SNR slope of D_2 for RIS-NOMA networks can be calculated as

$$S_{D_2}=\lim_{\rho\to\infty}\frac{R_{D_2}^{erg,\infty}(\rho)}{\log(\rho)}=0. \tag{46}$$

Remark 4.7. From Eq. (46), it can be observed that the high SNR slope of D_2 for RIS-NOMA is zero. This means that the ergodic rate of D_2 for RIS-NOMA is a constant. Hence the ergodic rate of D_2 for RIS-NOMA converges to a throughput ceiling at high SNR.

Similar to the derivation process of Eq. (37), the upper bound for the ergodic rate of D_n for RIS-OMA networks can be obtained in the following corollary.

Corollary 4.4. Under Rician fading channels, the upper bound for the ergodic rate of D_n for RIS-OMA is given by

$$R_{D_n,OMA}^{erg,UB}=\frac{1}{2}\log\left(1+\rho\left(\left(K\mu_n\right)^2+K\Omega_n\right)\right). \tag{47}$$

The asymptotic upper bound for the ergodic rate of D_n at high SNR for RIS-OMA networks can be provided in the following corollary.

Corollary 4.5. Based on Eq. (47), when $\rho\to\infty$, the asymptotic upper bound for the ergodic rate of D_n for RIS-OMA can be given by

$$R_{D_n,OMA}^{erg,UB,\infty}=\frac{1}{2}\log\left(\rho\left(\left(K\mu_n\right)^2+K\Omega_n\right)\right). \tag{48}$$

Remark 4.8. Substituting Eq. (48) into Eq. (36), the high SNR slope of D_n for RIS-OMA networks is equal to $\frac{1}{2}$.

4.5 Delay-Tolerant System Throughput

In the delay-tolerant transmission mode, the information is transmitted from the BS to users at any constant rate, which is subject to the channel conditions of the users. Hence the delay-tolerant system throughput of RIS-NOMA is expressed as

$$R_{DT}=R_{D_1}^{erg}+R_{D_2}^{erg}, \tag{49}$$

where $R_{D_1}^{erg}$ and $R_{D_2}^{erg}$ are the ergodic rates from Eqs. (31) and (33), respectively.

5 Numerical Results

In this section, numerical results are presented to evaluate the performance of RIS-NOMA networks over Rician fading channels. The effects of the Rician factor, the number of reflecting elements of the RIS, and the pass loss exponent on the performance of RIS-NOMA networks are discussed. The accuracy of the derived theoretical results can be verified by Monte Carlo simulations. In order to compare the performance with the RIS-NOMA networks, the conventional RIS-OMA networks are also provided. Without loss of generality, the power allocation factors of two users are set to $a_1 = 0.2$ and $a_2 = 0.8$, the target rates of two users are set to $r_1 = 0.0005$ bits per channel use (BPCU) and $r_2 = 0.002$ BPCU. In order to simplify the calculation, we adopt the normalized distance for dimensionless physical quantity. It is assumed that the distances from the BS to R_2 and from R_2 to D_2 are normalized to unity. The normalized distances from BS to R_1 and R_2, from R_1 to D_1, and from R_2 to D_2 are set to $d_{1,1} = 0.4$, $d_{2,1} = 0.5$, $d_{1,2} = 0.4$, and $d_{2,2} = 0.5$, respectively. For clarity, the main parameters used for numerical results are summarized in Table 1.

Table 1: The parameters for numerical results

Monte Carlo simulations repeated	10^6 iterations
The power allocation factors	$a_1 = 0.2$
	$a_2 = 0.8$
The targeted data rates	$r_1 = 0.0005$ BPCU
	$r_2 = 0.002$ BPCU
The normalized distances	$d_{1,1} = d_{1,2} = 0.4$
	$d_{2,1} = d_{2,2} = 0.5$
The path loss exponent	$\alpha = 2$

5.1 Outage Probability

Fig. 2 plots the outage probabilities of two users *vs.* the transmit SNR for RIS-NOMA networks. The parameters are set to $K = 8$, $\kappa = -10$ dB, and $\alpha = 2$. We can observe that the accurate outage probability curves given by Monte Carlo simulations are in good agreement with the derived theoretical outage probability results for RIS-NOMA networks, which verifies the accuracy of the derived theoretical outage probability results. It can be observed that the outage performance of RIS-NOMA networks is better than that of RIS-OMA networks. The reason is that RIS-NOMA can provide services for multiple users in the same time slot by adopting the superposition coding scheme, while RIS-OMA can only provide services for one user in each time slot. One can observe that the asymptotic outage probability curves converge to the derived theoretical results in the high SNR regime, which also demonstrates the accuracy of the theoretical analysis. As can be observed that the outage probability decreases with the increase of the transmit SNR. One can make the following observation from figure that the outage probabilities of two users converge to zeros in the high SNR regime and thus the non-zero diversity order can be obtained.

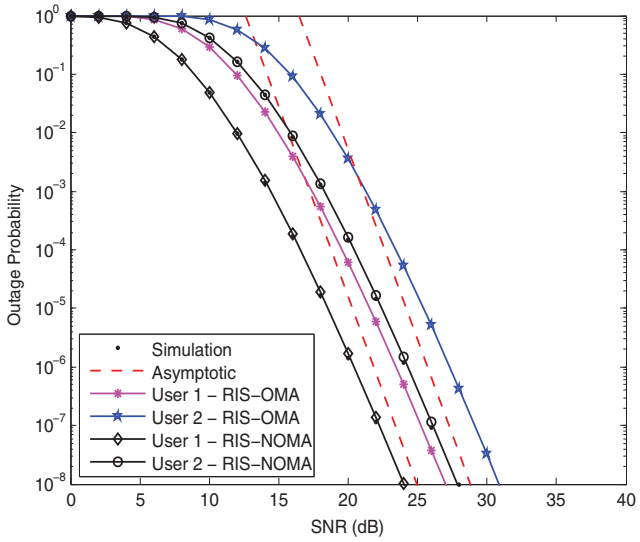

Figure 2: Outage probability *vs.* the transmit SNR when $K = 8$, $\kappa = -10$ dB, and $\alpha = 2$

Fig. 3 plots the outage probabilities of two users *vs.* the transmit SNR with different K for RIS-NOMA networks. The parameters are set to $\kappa = -10$ dB and $\alpha = 2$. It is observed that the outage probabilities of two users for RIS-NOMA decrease with increasing the number of reflecting elements K, thus the outage performance for RIS-NOMA can be improved. The reason is that the diversity orders of two users for RIS-NOMA depend on the number of reflecting elements.

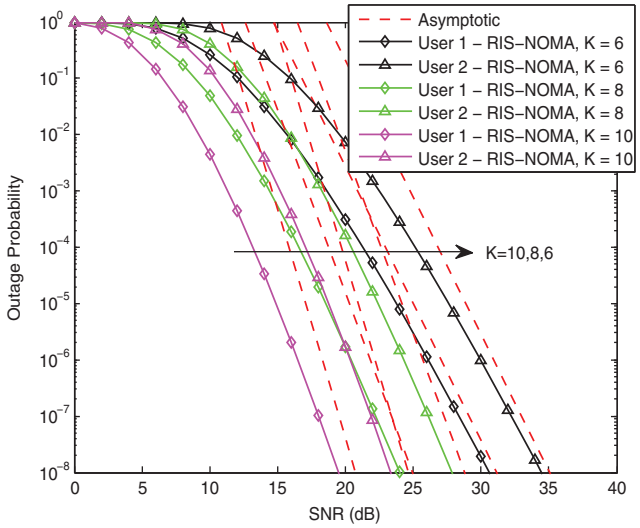

Figure 3: Outage probability *vs.* the transmit SNR with different K when $\kappa = -10$ dB and $\alpha = 2$

In order to explain the influence of the Rician factor on the outage performance of RIS-NOMA networks, Fig. 4 plots the outage probabilities of two users *vs.* the transmit SNR with different κ for RIS-NOMA networks. The parameters are set to $K = 8$ and $\alpha = 2$. As can be seen from the figure that as the value of the Rician factor κ increases, the outage probabilities of two users for RIS-NOMA reduce, hence the outage performance of RIS-NOMA becomes better. This is due to the fact that

the diversity orders of two users for RIS-NOMA are related to the value of the Rician factor. The reason behind this phenomenon is that there are a large number of LoS components of Rician fading channels, which greatly improves the outage performance of RIS-NOMA networks.

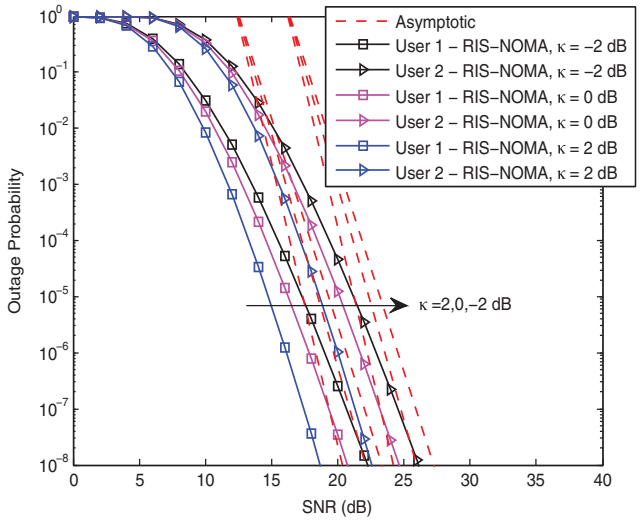

Figure 4: Outage probability *vs.* the transmit SNR with different κ when $K = 8$ and $\alpha = 2$

To further illustrate the impact of the path loss exponent on the outage performance of RIS-NOMA networks, Fig. 5 plots the outage probabilities of two users *vs.* the transmit SNR with different α for RIS-NOMA networks. The parameters are set to $K = 8$ and $\kappa = -10$ dB. It can be seen that the outage probabilities of two users for RIS-NOMA increase significantly with the decrease of the path loss exponent α, therefore the outage performance for RIS-NOMA deteriorates sharply. This is because that the path loss exponent reflects the number of obstacles in the propagation environment.

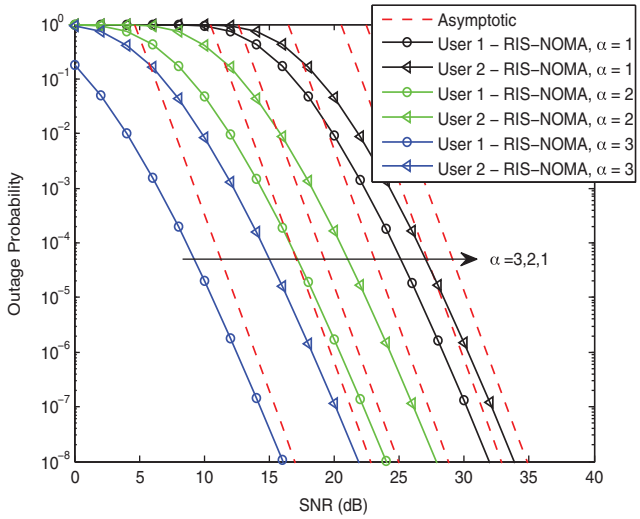

Figure 5: Outage probability *vs.* the transmit SNR with different α when $K = 8$ and $\kappa = -10$ dB

5.2 Ergodic Rate

Fig. 6 plots the ergodic rates of two users *vs.* the transmit SNR for RIS-NOMA networks. The parameters are set to $K = 20$, $\kappa = -10$ dB, and $\alpha = 2$. We can see from the figure that the Monte Carlo simulation ergodic rate curves are completely consistent with the derived theoretical ergodic rate results for RIS-NOMA, which demonstrates the accuracy of the derived theoretical ergodic rate results. Another observation is that the upper bound curve for ergodic rate of D_1 is very close to the derived theoretical ergodic rate. As can be observed from this figure that the ergodic rate of D_2 converges to a throughput ceiling at high SNR and therefore leads to a zero high SNR slope. The important observation is that the ergodic rate of D_1 for RIS-NOMA is higher than that of D_1 for RIS-OMA at high SNR. The reason is that the high SNR slope of D_1 for RIS-NOMA exceeds that of D_1 for RIS-OMA. On the other hand, the ergodic rate of D_2 for RIS-NOMA is lower than that of D_2 for RIS-OMA at high SNR. This is because that D_2 for RIS-NOMA has a smaller the high SNR slope compared with D_2 for RIS-OMA.

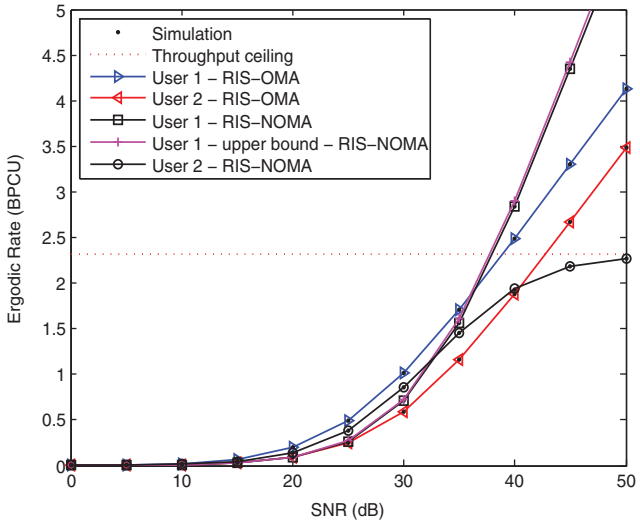

Figure 6: Ergodic rate *vs.* the transmit SNR when $K = 20$, $\kappa = -10$ dB, and $\alpha = 2$

Considering the influence of the number of reflecting elements on the ergodic performance of RIS-NOMA networks, Fig. 7 plots the ergodic rates of two users *vs.* the transmit SNR with different K for RIS-NOMA networks. The parameters are set to $\kappa = -10$ dB and $\alpha = 2$. We can observe from the figure that the ergodic rates of two users for RIS-NOMA increase as the number of reflecting elements K increases. Another observation is that the ergodic rate of D_1 is extremely large with respect to that of D_2 for RIS-NOMA with the increase of the number of reflecting elements. This is due to the fact that there is a throughput ceiling at high SNR for the ergodic rate of D_2 for RIS-NOMA.

5.3 System Throughput

Fig. 8 plots the system throughput *vs.* the transmit SNR with different K for RIS-NOMA networks in delay-limited transmission mode. The parameters are set to $\kappa = -10$ dB and $\alpha = 2$. It can be seen that RIS-NOMA is capable of enhancing the system throughput compared to RIS-OMA. The reason is that the system throughput depends on the outage probability in delay-limited transmission mode. One can make the following observation from figure that the system throughput of RIS-NOMA converges to a constant at high SNR. This phenomenon indicates that the system

throughput no longer increases with the increase of SNR when it reaches a fixed value at high SNR. Another observation is that as the number of reflecting elements increases, the system throughput of RIS-NOMA can be significantly improved.

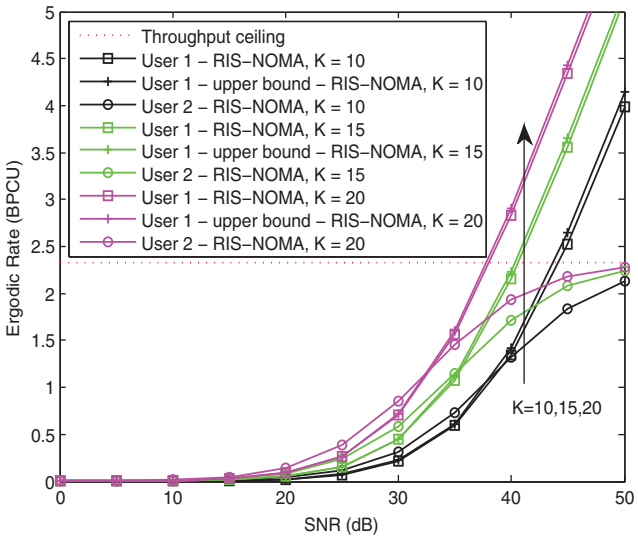

Figure 7: Ergodic rate *vs.* the transmit SNR with different K when $\kappa = -10$ dB and $\alpha = 2$

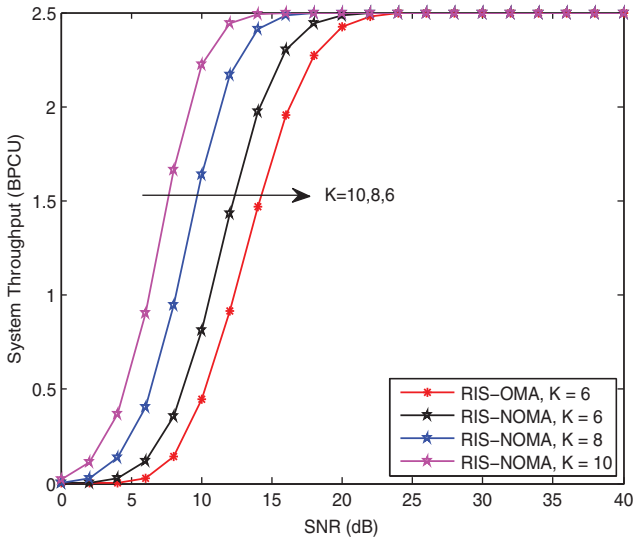

Figure 8: System throughput in delay-limited transmission mode *vs.* the transmit SNR with different K when $\kappa = -10$ dB and $\alpha = 2$

As a further advance, Fig. 9 plots the system throughput *vs.* the transmit SNR with different K for RIS-NOMA networks in delay-tolerant transmission mode. The parameters are set to $\kappa = -10$ dB and $\alpha = 2$. It can be observed that RIS-NOMA can achieve a larger system throughput than RIS-OMA at high SNR. The main reason behind this is that the system throughput is related to the ergodic rate in delay-tolerant transmission mode. It is observed from the figure that the system throughput of RIS-NOMA becomes larger with increasing the number of reflecting elements.

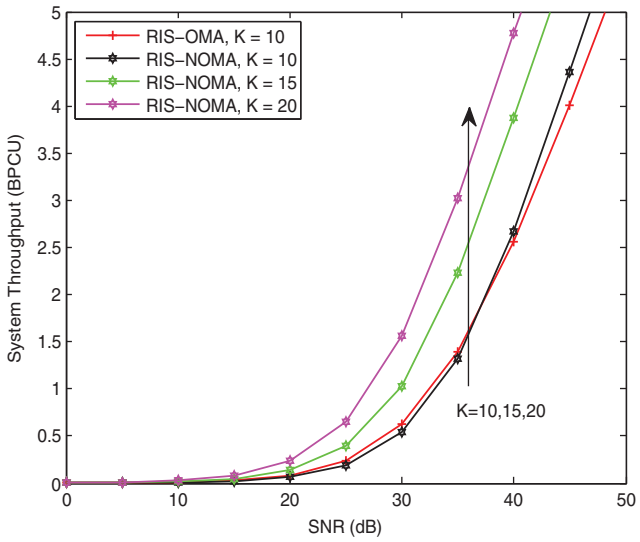

Figure 9: System throughput in delay-tolerant transmission mode *vs.* the transmit SNR with different K when $\kappa = -10$ dB and $\alpha = 2$

6 Conclusion

In this paper, the system performance of RIS-assisted downlink NOMA communication networks has been investigated in terms of the outage probability, ergodic rate, and system throughput over Rician fading channels. The exact and asymptotic expressions for the outage probability and ergodic rate of two users for RIS-NOMA networks have been derived. Based on the theoretical analyses, the diversity orders and high SNR slopes of the two users have been obtained at high SNR. In addition, the system throughputs of RIS-NOMA networks have been derived in delay-limited and delay-tolerant transmission modes. Simulation results have indicated that the outage probability and ergodic rate of RIS-NOMA outperform that of RIS-OMA. It has been shown that the system throughput of RIS-NOMA is superior to that of RIS-OMA. Moreover, it has been demonstrated that the system performance of RIS-NOMA networks becomes better with increasing the number of reflecting elements and Rician factor. Based on this work, we will consider extending the research to multiple users in the future. In addition, optimized power allocation and multiple antennas of device nodes are also promising research directions.

Funding Statement: This work was supported in part by the Key R&D Program of Zhejiang Province under Grant No. 2020C05005, in part by the National Natural Science Foundation of China under Grants U2033215, 91738301, 91538202, and 91638301, in part by the Program for New Century Excellent Talents in University under Grant NCET-09-0025, and in part by the Fundamental Research Funds for the Central Universities. The work of C. Huang was partially supported by the China National Key R&D Program under Grant 2021YFA1000500, National Natural Science Foundation of China under Grant 62101492, Zhejiang Provincial Natural Science Foundation of China under Grant LR22F010002, Distinguished Young Scholars of the National Natural Science Foundation of China, Ng Teng Fong Charitable Foundation in the form of ZJU-SUTD IDEA Grant, Zhejiang University Education Foundation Qizhen Scholar Foundation, and Fundamental Research Funds for the Central Universities under Grant 2021FZZX001-21. The work of X. Yue was supported by

the National Natural Science Foundation of China under Grant 62071052 and the R&D Program of Beijing Municipal Education Commission under Grant KM202011232003.

Conflicts of Interest: The authors declare that they have no conflicts of interest to report regarding the present study.

References

1. Ding, Z., Liu, Y., Choi, J., Sun, Q., Elkashlan, M. et al. (2017). Application of non-orthogonal multiple access in LTE and 5G networks. *IEEE Communications Magazine, 55(2),* 185–191. DOI 10.1109/MCOM.35.
2. Shirvanimoghaddam, M., Dohler, M., Johnson, S. J. (2017). Massive non-orthogonal multiple access for cellular IoT: Potentials and limitations. *IEEE Communications Magazine, 55(9),* 55–61. DOI 10.1109/MCOM.2017.1600618.
3. Liu, Y., Qin, Z., Elkashlan, M., Ding, Z., Nallanathan, A. et al. (2017). Non-orthogonal multiple access for 5G and beyond. *Proceedings of the IEEE, 105(12),* 2347–2381. DOI 10.1109/JPROC.2017.2768666.
4. Islam, S. M. R., Avazov, N., Dobre, O. A., Kwak, K. (2017). Power-domain non-orthogonal multiple access (NOMA) in 5G systems: Potentials and challenges. *IEEE Communications Surveys and Tutorials, 19(2),* 721–742. DOI 10.1109/COMST.2016.2621116.
5. Montalban, J., Scopelliti, P., Fadda, M., Iradier, E., Desogus, C. et al. (2018). Multimedia multicast services in 5G networks: Subgrouping and non-orthogonal multiple access techniques. *IEEE Communications Magazine, 56(3),* 91–95. DOI 10.1109/MCOM.2018.1700660.
6. Ding, Z., Yang, Z., Fan, P., Poor, H. V. (2014). On the performance of non-orthogonal multiple access in 5G systems with randomly deployed users. *IEEE Signal Processing Letters, 21(12),* 1501–1505. DOI 10.1109/LSP.97.
7. Yue, X., Qin, Z., Liu, Y., Kang, S., Chen, Y. (2018). A unified framework for non-orthogonal multiple access. *IEEE Transactions on Communications, 66(11),* 5346–5359. DOI 10.1109/TCOMM.2018.2842217.
8. Zhu, H., Wu, Q., Wu, X. J., Fan, Q., Fan, P. et al. (2022). Decentralized power allocation for MIMO-NOMA vehicular edge computing based on deep reinforcement learning. *IEEE Internet of Things Journal, 9(14),* 12770–12782. DOI 10.1109/JIOT.2021.3138434.
9. Liu, Y., Liu, X., Mu, X., Hou, T., Xu, J. et al. (2021). Reconfigurable intelligent surfaces: Principles and opportunities. *IEEE Communications Surveys and Tutorials, 23(3),* 1546–1577. DOI 10.1109/COMST.2021.3077737.
10. Zhang, Z., Xiao, Y., Ma, Z., Xiao, M., Ding, Z. et al. (2019). 6G wireless networks: Vision, requirements, architecture, and key technologies. *IEEE Vehicular Technology Magazine, 14(3),* 28–41. DOI 10.1109/MVT.10209.
11. Pan, C., Ren, H., Wang, K., Kolb, J. F., Elkashlan, M. et al. (2021). Reconfigurable intelligent surfaces for 6G systems: Principles, applications, and research directions. *IEEE Communications Magazine, 59(6),* 14–20. DOI 10.1109/MCOM.001.2001076.
12. Huang, C., Zappone, A., Alexandropoulos, G. C., Debbah, M., Yuen, C. (2019). Reconfigurable intelligent surfaces for energy efficiency in wireless communication. *IEEE Transactions on Wireless Communications, 18(8),* 4157–4170. DOI 10.1109/TWC.7693.
13. Huang, C., Hu, S., Alexandropoulos, G. C., Zappone, A., Yuen, C. et al. (2020). Holographic MIMO surfaces for 6G wireless networks: Opportunities, challenges, and trends. *IEEE Wireless Communications, 27(5),* 118–125. DOI 10.1109/MWC.7742.
14. Zhou, G., Pan, C., Ren, H., Wang, K., Nallanathan, A. (2020). A framework of robust transmission design for IRS-aided MISO communications with imperfect cascaded channels. *IEEE Transactions on Signal Processing, 68,* 5092–5106. DOI 10.1109/TSP.2020.3019666.

15. Wu, Q., Zhang, R. (2020). Towards smart and reconfigurable environment: Intelligent reflecting surface aided wireless network. *IEEE Communications Magazine, 58(1),* 106–112. DOI 10.1109/MCOM.35.
16. Wei, L., Huang, C., Alexandropoulos, G. C., Yuen, C., Zhang, Z. et al. (2021). Channel estimation for RIS-empowered multi-user MISO wireless communications. *IEEE Transactions on Communications, 69(6),* 4144–4157. DOI 10.1109/TCOMM.2021.3063236.
17. Yang, Z., Chen, M., Saad, W., Xu, W., Shikh-Bahaei, M. et al. (2022). Energy-efficient wireless communications with distributed reconfigurable intelligent surfaces. *IEEE Transactions on Wireless Communications, 21(1),* 665–679. DOI 10.1109/TWC.2021.3098632.
18. Huang, C., Mo, R., Yuen, C. (2020). Reconfigurable intelligent surface assisted multiuser MISO systems exploiting deep reinforcement learning. *IEEE Journal on Selected Areas in Communications, 38(8),* 1839–1850. DOI 10.1109/JSAC.49.
19. Yang, Z., Xu, W., Huang, C., Shi, J., Shikh-Bahaei, M. (2021). Beamforming design for multiuser transmission through reconfigurable intelligent surface. *IEEE Transactions on Communications, 69(1),* 589–601. DOI 10.1109/TCOMM.26.
20. Huang, C., Yang, Z., Alexandropoulos, G. C., Xiong, K., Wei, L. et al. (2021). Multi-hop RIS-empowered terahertz communications: A DRL-based hybrid beamforming design. *IEEE Journal on Selected Areas in Communications, 39(6),* 1663–1677. DOI 10.1109/JSAC.2021.3071836.
21. Ding, Z., Poor, H. V. (2020). A simple design of IRS-NOMA transmission. *IEEE Communications Letters, 24(5),* 1119–1123. DOI 10.1109/COML.4234.
22. Yue, X., Liu, Y. (2022). Performance analysis of intelligent reflecting surface assisted NOMA networks. *IEEE Transactions on Wireless Communications, 21(4),* 2623–2636. DOI 10.1109/TWC.2021.3114221.
23. Ding, Z., Schober, R., Poor, H. V. (2020). On the impact of phase shifting designs on IRS-NOMA. *IEEE Wireless Communication Letters, 9(10),* 1596–1600. DOI 10.1109/LWC.5962382.
24. Hou, T., Liu, Y., Song, Z., Sun, X., Chen, Y. et al. (2020). Reconfigurable intelligent surface aided NOMA networks. *IEEE Journal on Selected Areas in Communications, 38(11),* 2575–2588. DOI 10.1109/JSAC.49.
25. Zheng, B., Wu, Q., Zhang, R. (2020). Intelligent reflecting surface-assisted multiple access with user pairing: NOMA or OMA? *IEEE Communications Letters, 24(4),* 753–757. DOI 10.1109/COML.4234.
26. Khaleel, A., Basar, E. (2022). A novel NOMA solution with RIS partitioning. *IEEE Journal of Selected Topics in Signal Processing, 16(1),* 70–81. DOI 10.1109/JSTSP.2021.3127725.
27. Cheng, Y., Li, K. H., Liu, Y., Teh, K. C., Karagiannidis, G. K. (2021). Non-orthogonal multiple access (NOMA) with multiple intelligent reflecting surfaces. *IEEE Transactions on Wireless Communications, 20(11),* 7184–7195. DOI 10.1109/TWC.2021.3081423.
28. Hemanth, A., Umamaheswari, K., Pogaku, A. C., Do, D. T., Lee, B. M. (2020). Outage performance analysis of reconfigurable intelligent surfaces-aided NOMA under presence of hardware impairment. *IEEE Access, 8,* 212156–212165. DOI 10.1109/Access.6287639.
29. Cheng, Y., Li, K. H., Liu, Y., Teh, K. C., Vincent Poor, H. (2021). Downlink and uplink intelligent reflecting surface aided networks: NOMA and OMA. *IEEE Transactions on Wireless Communications, 20(6),* 3988–4000. DOI 10.1109/TWC.2021.3054841.
30. Gong, X., Huang, C., Yue, X., Liu, F., Yang, Z. (2022). Performance analysis for reconfigurable intelligent surface assisted downlink NOMA networks. *IET Communications, 16(13),* 1593–1605. DOI 10.1049/cmu2.12375.
31. Simon, M. K. (2006). *Probability distributions involving gaussian random variables*. USA: Springer.
32. Gradshteyn, I. S., Ryzhik, I. M. (2000). *Table of integrals, series and products*. 6th edition. New York, NY, USA: Academic Press.
33. Primak, S., Kontorovitch, V., Lyandres, V. (2004). *Stochastic methods and their applications to communications: Stochastic differential equations approach*. West Sussex, UK: Wiley.
34. Hildebrand, B. F. (1987). *Introduction to numerical analysis*. New York, NY, USA: Dover.

Appendix A: Proof of Theorem 1

Substituting Eqs. (7) and (8) into Eq. (16), based on Eq. (12), the outage probability of D_1 for RIS-NOMA networks is expressed as

$$\begin{aligned} P_{D_1} &= 1 - \Pr\left(\left|\mathbf{H}_1^H \vartheta_1 \mathbf{G}_1\right|^2 > \lambda_1, \left|\mathbf{H}_1^H \vartheta_1 \mathbf{G}_1\right|^2 > \lambda_2\right) \\ &= 1 - \Pr\left(\left|\mathbf{H}_1^H \vartheta_1 \mathbf{G}_1\right|^2 > \max(\lambda_1, \lambda_2)\right) \\ &= 1 - \Pr\left(\left|\mathbf{H}_1^H \vartheta_1 \mathbf{G}_1\right|^2 > \lambda\right) \\ &= \Pr\left(\sum_{k=1}^{K} \left|G_1^k H_1^k\right| < \sqrt{\lambda}\right), \end{aligned} \tag{A.1}$$

where $\lambda \triangleq \max(\lambda_1, \lambda_2)$, $\lambda_1 = \dfrac{\gamma_{th_1}}{\rho a_1}$, and $\lambda_2 = \dfrac{\gamma_{th_2}}{\rho(a_2 - a_1\gamma_{th_2})}$ with $a_2 > a_1\gamma_{th_2}$.

Applying the series of Laguerre polynomials [33], the PDF of $X_1 = \sum_{k=1}^{K} \left|G_1^k H_1^k\right|$ is approximated as

$$f_{X_1}(x) \approx \frac{x^{\omega_1}}{(\upsilon_1)^{\omega_1+1}\Gamma(\omega_1+1)} \exp\left(-\frac{x}{\upsilon_1}\right), \tag{A.2}$$

where $\omega_1 = \dfrac{K\mu_1^2}{\Omega_1} - 1$ and $\upsilon_1 = \dfrac{\Omega_1}{\mu_1}$.

Substituting Eq. (A.2) into Eq. (A.1), the outage probability of D_1 can be approximated as

$$\begin{aligned} P_{D_1} &= \Pr\left(X_1 < \sqrt{\lambda}\right) \\ &\approx \int_0^{\sqrt{\lambda}} \frac{x^{\omega_1}}{(\upsilon_1)^{\omega_1+1}\Gamma(\omega_1+1)} \exp\left(-\frac{x}{\upsilon_1}\right) dx \\ &= \frac{1}{(\upsilon_1)^{\omega_1+1}\Gamma(\omega_1+1)} \int_0^{\sqrt{\lambda}} x^{\omega_1} \mathrm{e}^{-\frac{x}{\upsilon_1}} dx. \end{aligned} \tag{A.3}$$

Using $t = \dfrac{x}{\upsilon_1}$, the outage probability of D_1 is expressed as

$$P_{D_1} \approx \frac{1}{\Gamma(\omega_1+1)} \int_0^{\frac{\sqrt{\lambda}}{\upsilon_1}} t^{\omega_1} \mathrm{e}^{-t} dt. \tag{A.4}$$

Applying the lower incomplete Gamma function [32], the outage probability of D_1 can be calculated as

$$\begin{aligned} P_{D_1} &\approx \frac{1}{\Gamma(\omega_1+1)} \int_0^{\frac{\sqrt{\lambda}}{\upsilon_1}} t^{(\omega_1+1)-1} \mathrm{e}^{-t} dt \\ &= \frac{1}{\Gamma(\omega_1+1)} \gamma\left(\omega_1+1, \frac{\sqrt{\lambda}}{\upsilon_1}\right) \end{aligned}$$

$$= \frac{1}{\Gamma\left(\frac{K\mu_1^2}{\Omega_1}\right)}\gamma\left(\frac{K\mu_1^2}{\Omega_1}, \frac{\mu_1\sqrt{\lambda}}{\Omega_1}\right), \tag{A.5}$$

where $\Omega_1 = \alpha_{1,1}\alpha_{1,2}\left\{1 - \frac{\pi^2}{16(1+\kappa)^2}\left[L_{\frac{1}{2}}(-\kappa)\right]^4\right\}$ and $\mu_1 = \frac{\pi\sqrt{\alpha_{1,1}\alpha_{1,2}}}{4(1+\kappa)}\left[L_{\frac{1}{2}}(-\kappa)\right]^2$. Thus, Eq. (17) can be obtained. The proof is completed.

Appendix B: Proof of Theorem 2

Substituting Eq. (9) into Eq. (18), the outage probability of D_2 for RIS-NOMA networks can be expressed as

$$\begin{aligned} P_{D_2} &= \Pr\left(\frac{\rho\left|\mathbf{H}_2^H\vartheta_2\mathbf{G}_2\right|^2 a_2}{\rho\left|\mathbf{H}_2^H\vartheta_2\mathbf{G}_2\right|^2 a_1 + 1} < \gamma_{th_2}\right) \\ &= \Pr\left(\left|\mathbf{H}_2^H\vartheta_2\mathbf{G}_2\right|^2 < \lambda_2\right) \\ &= \Pr\left(\sum_{k=1}^{K}\left|G_2^k H_2^k\right| < \sqrt{\lambda_2}\right), \end{aligned} \tag{B.1}$$

where the last equality holds because of Eq. (12).

Similarly, the PDF of $X_2 = \sum_{k=1}^{K}\left|G_2^k H_2^k\right|$ by utilizing the series of Laguerre polynomials can be approximated as

$$f_{X_2}(x) \approx \frac{x^{\omega_2}}{(\upsilon_2)^{\omega_2+1}\Gamma(\omega_2+1)}\exp\left(-\frac{x}{\upsilon_2}\right), \tag{B.2}$$

where $\omega_2 = \frac{K\mu_2^2}{\Omega_2} - 1$ and $\upsilon_2 = \frac{\Omega_2}{\mu_2}$.

Substituting Eq. (B.2) into Eq. (B.1), using $u = \frac{x}{\upsilon_2}$, the outage probability of D_2 can be approximated as

$$\begin{aligned} P_{D_2} &= \Pr\left(X_2 < \sqrt{\lambda_2}\right) \\ &\approx \int_0^{\sqrt{\lambda_2}} \frac{x^{\omega_2}}{(\upsilon_2)^{\omega_2+1}\Gamma(\omega_2+1)}\exp\left(-\frac{x}{\upsilon_2}\right)dx \\ &= \frac{1}{\Gamma(\omega_2+1)}\int_0^{\frac{\sqrt{\lambda_2}}{\upsilon_2}} u^{\omega_2}\mathrm{e}^{-u}du. \end{aligned} \tag{B.3}$$

By referring to the lower incomplete Gamma function, the outage probability of D_2 can be calculated as

$$P_{D_2} \approx \frac{1}{\Gamma(\omega_2+1)}\gamma\left(\omega_2+1, \frac{\sqrt{\lambda_2}}{\upsilon_2}\right) = \frac{1}{\Gamma\left(\frac{K\mu_2^2}{\Omega_2}\right)}\gamma\left(\frac{K\mu_2^2}{\Omega_2}, \frac{\mu_2\sqrt{\lambda_2}}{\Omega_2}\right), \tag{B.4}$$

where $\mu_2 = \frac{\pi\sqrt{\alpha_{2,1}\alpha_{2,2}}}{4(1+\kappa)}\left[L_{\frac{1}{2}}(-\kappa)\right]^2$ and $\Omega_2 = \alpha_{2,1}\alpha_{2,2}\left\{1 - \frac{\pi^2}{16(1+\kappa)^2}\left[L_{\frac{1}{2}}(-\kappa)\right]^4\right\}$. Hence Eq. (19) can be obtained. The proof is completed.

Appendix C: Proof of Theorem 3

Substituting Eq. (8) into Eq. (30), according to Eq. (12), the ergodic rate of D_1 for RIS-NOMA networks can be expressed as

$$\begin{aligned} R_{D_1}^{erg} &= \mathbb{E}\left[\log\left(1 + \left|\mathbf{H}_1^H \vartheta_1 \mathbf{G}_1\right|^2 \rho a_1\right)\right] \\ &= \mathbb{E}\left[\log\left(1 + \underbrace{\left|\sum_{k=1}^{K}\left|G_1^k H_1^k\right|\right|^2}_{Y_1}\rho a_1\right)\right] \\ &= \frac{\rho a_1}{\ln 2}\int_0^{\infty}\frac{1 - F_{Y_1}(y)}{1+\rho a_1 y}dy. \end{aligned} \tag{C.1}$$

The CDF of Y_1 can be written as

$$F_{Y_1}(y) = \Pr\left(\left|\sum_{k=1}^{K}\left|G_1^k H_1^k\right|\right|^2 < y\right) = \Pr\left(X_1 < \sqrt{y}\right). \tag{C.2}$$

Based on Eq. (17), the CDF of Y_1 is given by

$$F_{Y_1}(y) \approx \frac{1}{\Gamma(\omega_1+1)}\gamma\left(\omega_1 + 1, \frac{\sqrt{y}}{\upsilon_1}\right). \tag{C.3}$$

Substituting Eq. (C.3) into Eq. (C.1), the ergodic rate of D_1 can be approximated as

$$R_{D_1}^{erg} \approx \frac{\rho a_1}{\ln 2}\int_0^{\infty}\frac{\Gamma(\omega_1+1) - \gamma\left(\omega_1+1, \frac{\sqrt{y}}{\upsilon_1}\right)}{(1+\rho a_1 y)\Gamma(\omega_1+1)}dy. \tag{C.4}$$

Hence Eq. (31) can be obtained. The proof is completed.

Appendix D: Proof of Theorem 4

Substituting Eq. (9) into Eq. (32), in view of Eq. (12), the ergodic rate of D_2 for RIS-NOMA networks can be expressed as

$$\begin{aligned} R_{D_2}^{erg} &= \mathbb{E}\left[\log\left(1 + \frac{\rho\left|\mathbf{H}_2^H \vartheta_2 \mathbf{G}_2\right|^2 a_2}{\rho\left|\mathbf{H}_2^H \vartheta_2 \mathbf{G}_2\right|^2 a_1 + 1}\right)\right] \\ &= \mathbb{E}\left[\log\left(1 + \underbrace{\frac{\rho\left|\sum_{k=1}^{K}\left|G_2^k H_2^k\right|\right|^2 a_2}{\rho\left|\sum_{k=1}^{K}\left|G_2^k H_2^k\right|\right|^2 a_1 + 1}}_{Y_2}\right)\right] \end{aligned}$$

$$= \frac{1}{\ln 2}\int_0^{\infty} \frac{1 - F_{Y_2}(y)}{1+y} dy. \tag{D.1}$$

The CDF of Y_2 can be written as

$$\begin{aligned} F_{Y_2}(y) &= \Pr\left(\frac{\rho \left|\sum_{k=1}^{K} \left|G_2^k H_2^k\right|\right|^2 a_2}{\rho \left|\sum_{k=1}^{K} \left|G_2^k H_2^k\right|\right|^2 a_1 + 1} < y \right) \\ &= \Pr\left(\left| \sum_{k=1}^{K} \left|G_2^k H_2^k\right| \right|^2 < \frac{y}{\rho(a_2 - a_1 y)} \right) \\ &= \Pr\left(X_2 < \sqrt{\frac{y}{\rho(a_2 - a_1 y)}} \right), \end{aligned} \tag{D.2}$$

where $a_2 > a_1 y$. According to Eq. (19), the CDF of Y_2 can be given by

$$F_{Y_2}(y) \approx \frac{1}{\Gamma(\omega_2 + 1)} \gamma\left(\omega_2 + 1, \frac{1}{\upsilon_2}\sqrt{\frac{y}{\rho(a_2 - a_1 y)}}\right). \tag{D.3}$$

Substituting Eq. (D.3) into Eq. (D.1), the ergodic rate of D_2 can be approximated as

$$R_{D_2}^{erg} \approx \frac{1}{\ln 2}\int_0^{\frac{a_2}{a_1}} \frac{1}{1+y}\left[1 - \frac{1}{\Gamma(\omega_2 + 1)} \gamma\left(\omega_2 + 1, \frac{1}{\upsilon_2}\sqrt{\frac{y}{\rho(a_2 - a_1 y)}}\right)\right] dy. \tag{D.4}$$

Using $t = 2\left(\frac{a_1}{a_2}\right) y - 1$, the ergodic rate of D_2 is expressed as

$$R_{D_2}^{erg} \approx \frac{1}{\ln 2}\int_{-1}^{1} \frac{a_2}{2a_1 + a_2(t+1)}\left[1 - \frac{1}{\Gamma(\omega_2 + 1)} \gamma\left(\omega_2 + 1, \frac{1}{\upsilon_2}\sqrt{\frac{t+1}{\rho a_1(1-t)}}\right)\right] dt. \tag{D.5}$$

Applying Chebyshev-Gauss quadrature [34], the ergodic rate of D_2 can be calculated as

$$R_{D_2}^{erg} \approx \frac{\pi}{L \ln 2} \sum_{l=1}^{L} \frac{a_2\sqrt{1 - t_l^2}}{2a_1 + a_2(t_l + 1)}\left[1 - \frac{1}{\Gamma(\omega_2 + 1)} \gamma\left(\omega_2 + 1, \frac{1}{\upsilon_2}\sqrt{\frac{t_l + 1}{\rho a_1(1 - t_l)}}\right)\right], \tag{D.6}$$

where $t_l = \cos\left(\frac{2l-1}{2L}\pi\right)$. Hence Eq. (33) can be obtained. The proof is completed.